ACS OMEGA

http://pubs.acs.org/journal/acsodf

Article

# Dwell Time Prolongation and Identification of Single Nucleotides Passing through a Solid-State Nanopore by Using Ammonium Sulfate Aqueous Solution

Itaru Yanagi,* Rena Akahori, and Ken-ichi Takeda

Cite This: *ACS Omega* 2023, 8, 21285−21292

Read Online

ACCESS | Metrics & More | Article Recommendations | Supporting Information

**ABSTRACT:** The ionic current blockades when poly(dT)$_{60}$ or dNTPs passed through SiN nanopores in an aqueous solution containing $(NH_4)_2SO_4$ were investigated. The dwell time of poly(dT)$_{60}$ in the nanopores in an aqueous solution containing $(NH_4)_2SO_4$ was significantly longer compared to that in an aqueous solution that did not contain $(NH_4)_2SO_4$. This dwell time prolongation effect due to the aqueous solution containing $(NH_4)_2SO_4$ was also confirmed when dCTP passed through the nanopores. In addition, when the nanopores were fabricated via dielectric breakdown in the aqueous solution containing $(NH_4)_2SO_4$, the dwell time prolongation effect for dCTP still occurred even after the aqueous solution was displaced with the aqueous solution without $(NH_4)_2SO_4$. Furthermore, we measured the ionic current blockades when the four types of dNTPs passed through the same nanopore, and the four types of dNTPs could be statistically identified according to their current blockade values.

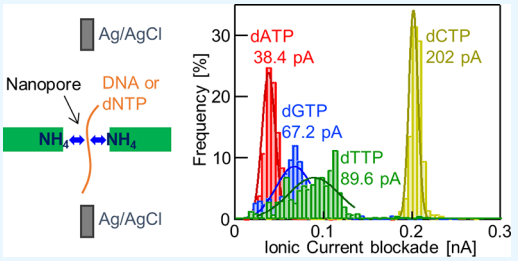


## 1. INTRODUCTION

In recent years, nanopores have been widely used as powerful probes to detect various biomolecules in aqueous solution. The structural and electrical properties of molecules can be determined by monitoring the change in ionic current when the molecule passes through a nanopore. The most noticeable application of nanopore sensing is label-free single-molecule DNA sequencing, which was achieved by using nanopores formed from biological molecules (i.e., biological nanopores).[1−4] Currently, a rich line up of nanopore DNA sequencers is being commercialized by Oxford Nanopore Technologies, Ltd., and many researchers can use them.[5−10] In addition to biological nanopores, solid-state nanopores (SSNs) formed from inorganic materials, which are the focus of this study, have been well studied,[11−21] and many papers have reported that SSNs are somewhat capable of single-molecule identification.[22−26] SSNs are advantageous in terms of robustness and material stability. However, DNA sequencing has not been achieved with SSNs although there are some simulation studies that suggested the possibility of DNA sequencing with SSNs.[27,28]

One of the key challenges in realizing DNA sequencing with SSNs is reducing the speed of DNA molecules passing through a nanopore. When single-stranded DNA (ssDNA) passes through a nanopore by electrophoretic force, the dwell time of ssDNA in the nanopore is usually less than 1 $\mu$s/base; it is difficult to precisely measure the current change in such a short time. (At least, it is almost impossible with commercially available amplifiers.) Therefore, many efforts have been devoted to decelerating DNA translocation through a nanopore. For instance, the solution characteristics, such as viscosity,[29] temperature,[30,31] type of solute,[32,33] and gradient concentration of solute,[34] were adjusted to reduce the speed of DNA. In addition, decreasing the nanopore size[31,35] and using $HfO_2$[36] as the nanopore material were shown to be effective methods for decelerating DNA translocation through nanopores. Furthermore, placing an obstacle, such as silica beads,[37] a nanofiber mesh,[38,39] a polymer gel,[40] or a self-assembled polyethylene-oxide film[41] on the nanopore membrane also slowed the speed of DNA. In addition to the above approaches of developing solutions and nanopore membrane structures, the direct control of DNA motion was also studied. For instance, optical tweezers,[42] magnetic tweezers,[43] or piezo actuators[44,45] were used to directly control the motion of DNA in nanopores.

Studies on the speed of DNA passing through a nanopore were also conducted with biological nanopores. Recently, Wang et al. reported that the speed of DNA was reduced by modifying the inner wall surface of an aerolysin nanopore.[46] Their report suggested that amino groups on the inner wall surface had a significant influence on the speed of DNA. Inspired by this report, in this study, we examined ssDNA (poly(dT)$_{60}$) translocation through a SiN nanopore in an

**Received:** April 20, 2023
**Accepted:** May 22, 2023
**Published:** June 1, 2023

aqueous solution containing $(NH_4)_2SO_4$. As a result, the translocation speed of poly(dT)$_{60}$ was found to be slower than that in an aqueous solution that did not contain $(NH_4)_2SO_4$. Similarly, the translocation speed of a DNA monomer (dCTP) was also found to be significantly slowed in an aqueous solution containing $(NH_4)_2SO_4$. Furthermore, we measured the ionic current blockades when the four types of dNTPs passed through the same nanopore and found that the four dNTPs could be statistically identified according to their current blockade values.

## 2. EXPERIMENTAL DETAILS

The membrane chip used for nanopore measurements is illustrated in Figure 1a. A 5 nm-thick SiN membrane was fabricated by using the poly-Si sacrificial layer process, the details of which are described elsewhere.[47,48] Before the measurements, the chip was cleaned and hydrophilized with piranha solution ($H_2O_2$:$H_2SO_4$ = 1:3) for 3 min and assembled into an acrylic flow cell (Figure 1b). The flow cell had two chambers (each with a volume of 90 $\mu$L) separated by the membrane: a *cis* chamber and a *trans* chamber. Each chamber was filled with electrolyte solution. In this study, two types of solutions were used: an aqueous solution consisting of 1 M KCl and 10 mM Tris−HCl at pH 7.5 and another aqueous solution consisting of 0.5 M KCl, 0.5 M $(NH_4)_2SO_4$, and 10 mM Tris−HCl at pH 7.5. After filling the aqueous solution into both chambers, two Ag/AgCl electrodes were immersed in both solutions to ensure electrical contact. We did not use a $(NH_4)_2SO_4$ aqueous solution without KCl because it does not conduct current with Ag/AgCl electrodes.

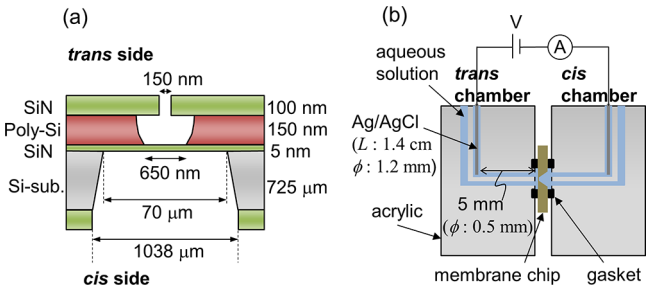


**Figure 1.** (a) Cross-sectional schematic of a membrane chip fabricated using the poly-Si sacrificial layer process. (b) Schematic illustration of the nanopore measurement setup.

A nanopore was fabricated in the membrane by using multilevel pulse-voltage injection (MPVI)[49] with a 4156B Precision Semiconductor Analyzer (Agilent Technologies, Inc., Santa Clara, CA, USA) and a 41501B SMU and Pulse Generator Expander (Agilent Technologies, Inc., Santa Clara, CA, USA). The pulse voltage for nanopore generation was set at 5−6 V with a duration of 1 ms−1 s. The duration of the $n_{th}$ voltage pulse ($t_n$) was set as

$$t_n = 10^{-3+(n-1)/N} - 10^{-3+(n-2)/N} \text{ [s] for } n \geq 2$$

$$t_1 = 10^{-3} \text{ [s] for } n = 1 \quad (1)$$

where $N$ was set at 12. The generated nanopores were widened to the desired size by applying additional voltage pulses, which were approximately half the magnitude of the first voltage pulses used for nanopore generation.

The diameters of the fabricated nanopores were estimated from the open pore current ($I_o$) using the following equation:

$$I_o = V\sigma\left(\frac{4h_{eff}}{\pi d^2} + \frac{1}{d}\right)^{-1} \quad (2)$$

where $V$ is the applied voltage, $h_{eff}$ is the effective height of the nanopore, $d$ is the diameter of the nanopore, and $\sigma$ is the measured conductance of the solutions: $\sigma$ = 0.1028 S/cm for the 1 M KCl buffer solution at 23 °C, and $\sigma$ = 0.116 S/cm for the 0.5 M KCl + 0.5 M $(NH_4)_2SO_4$ buffer solution at 23 °C. According to several previous reports,[47,49,50] $h_{eff}$ can be approximately estimated as one-third of the actual thickness

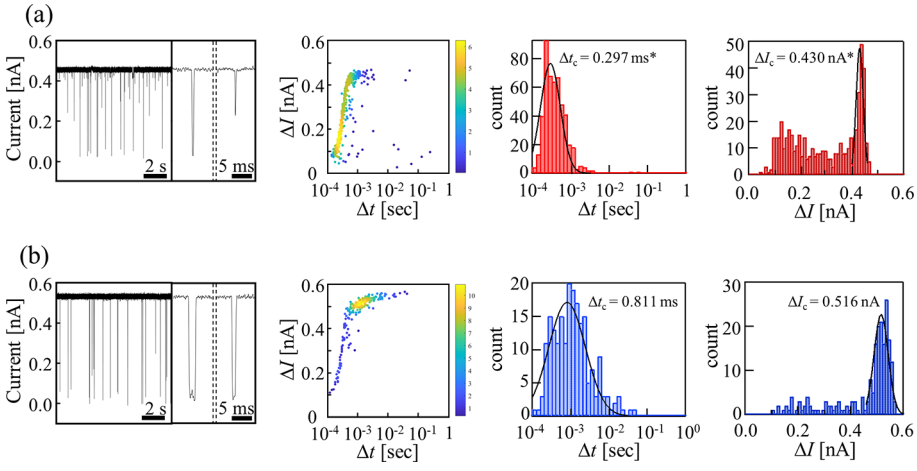


**Figure 2.** Ionic current blockades at 0.1 V when poly(dT)$_{60}$ passed through nanopores. Each data set includes a time trace of the ionic current, a kernel density scatter plot of the ionic current blockade values ($\Delta I$) and dwell times ($\Delta t$), and histograms of $\Delta t$ and $\Delta I$. The histograms were fitted with Gaussian functions, and their central values were determined to be $\Delta t_C$ and $\Delta I_C$. (a) Data set of ionic current blockades when the nanopore formation and current blockade measurement were performed in a 1 M KCl aqueous solution. (b) Data set of ionic current blockades when the nanopore formation and current blockade measurement were performed in a 0.5 M KCl + 0.5 M $(NH_4)_2SO_4$ aqueous solution. *Note that the statics that rely on many events with a $\Delta t$ of less than 0.5 ms are less reliable because the current was low-pass filtered with a cutoff frequency of 2 kHz. Especially, the data in (a) is derived from many events with a $\Delta t$ of less than 0.5 ms, and the values of $\Delta t_C$ and $\Delta I_C$ with asterisks in (a) are less accurate than the others.



https://doi.org/10.1021/acsomega.3c02703
ACS Omega 2023, 8, 21285−21292

of the SiN membrane. However, our previous study[51] showed that $h_{eff}$ does not vary much from the actual membrane thickness when the actual membrane thickness is less than 6 nm. Therefore, in this study, $h_{eff}$ was set as the actual membrane thickness (i.e., 5 nm).

After the nanopore was fabricated, the aqueous solution in the *cis* chamber was displaced with the 1 M KCl or 0.5 M KCl + 0.5 M $(NH_4)_2SO_4$ buffer solution containing 5 nM poly(dT)$_{60}$ (Integrated DNA Technologies, Inc.) or 100 $\mu$M dNTPs (Thermo Fisher Scientific Inc.). Then, the ionic current through the nanopore was measured using a patch-clamp amplifier (Axopatch 200B, Axon Instruments, Union City, CA). The detected current was low-pass filtered with a cutoff frequency of 2 kHz using a four-pole Bessel filter and then digitized with an NI USB-6281 18-bit DAQ AD converter (National Instruments, Austin, TX) at 50 kHz. Finally, the current was recorded on the hard disk of a personal computer. All the measurements described above were performed at room temperature.

## 3. RESULTS AND DISCUSSION

Figure 2 presents the data set of ionic current blockades when poly(dT)$_{60}$ passed through the nanopores. The voltage applied was 0.1 V. Figure 2a shows the data when the nanopore formation and current blockade measurement were performed in the 1 M KCl aqueous solution. Figure 2b shows the data when the nanopore formation and current blockade measurement were performed in the 0.5 M KCl + 0.5 M $(NH_4)_2SO_4$ aqueous solution. The time trace of the ionic current, the scatter plot of the ionic current blockade values ($\Delta I$) and dwell times ($\Delta t$), and the histograms of $\Delta I$ and $\Delta t$ are shown in each figure. The sizes of the two types of nanopores used in the two experiments were almost the same: the nanopore diameters estimated from eq 2 were 1.92 nm (used to collect the experimental data shown in Figure 2a) and 1.97 nm (used to collect the experimental data shown in Figure 2b).

The time traces of the ionic currents in both figures indicated clear ionic current blockades regardless of whether $(NH_4)_2SO_4$ was present in the KCl aqueous solution. Regarding the dwell time, longer dwell time events were observed when $(NH_4)_2SO_4$ was present in the KCl aqueous solution (refer to the scatter plot and $\Delta t$ histogram in each figure). The histograms of $\Delta t$ and $\Delta I$ were fitted with Gaussian functions, and their central values were determined as $\Delta t_C$ and $\Delta I_C$. $\Delta t_C$ with $(NH_4)_2SO_4$ and $\Delta t_C$ without $(NH_4)_2SO_4$ were 0.811 and 0.297 ms, respectively. Goto et al. reported that some types of cations generated by salt dissolution were adsorbed onto silanol groups on the wall of a SiN nanopore, and the dwell time of DNA passing through the nanopore was increased by the interactions between the adsorbed cations and DNA.[25] Therefore, one possible reason for this longer $\Delta t$ with $(NH_4)_2SO_4$ could be the interactions between poly(dT)$_{60}$ and $NH_4^+$, which was adsorbed on the silanol groups of the nanopore wall surface. Regarding the current blockade values, $\Delta I_C$ with $(NH_4)_2SO_4$ (=0.516 nA) was approximately 1.2 times larger than $\Delta I_C$ without $(NH_4)_2SO_4$ (=0.430 nA). One of the reasons for this difference could be the difference in conductance between the aqueous solutions: the ratio of $\sigma$(0.5 M KCl + 0.5 M $(NH_4)_2SO_4$) = 0.116 S/cm to $\sigma$(1 M KCl) = 0.1028 S/cm was 1.13.

To confirm the reproducibility of the dwell time prolongation of poly(dT)$_{60}$ passing through nanopores, the same experiment was performed multiple times with different-sized nanopores. The dependence of $\Delta t_C$ on the nanopore diameter is shown in Figure 3. Eight data points were obtained

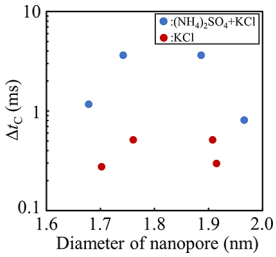


**Figure 3.** Dependence of $\Delta t_C$ on the nanopore diameter when poly(dT)$_{60}$ passed through nanopores at 0.1 V. Eight different nanopores were used for the measurement. The blue symbols represent the data measured using a 0.5 M KCl + 0.5 M $(NH_4)_2SO_4$ aqueous solution. The red symbols represent the data measured using a 1 M KCl aqueous solution.

from measurements using eight different nanopores with diameters of 1.68−1.97 nm. The scatter plot and histograms of $\Delta t$ and $\Delta I$ for each data point are shown in Figure S1 in the Supporting Information, except for the data already presented in Figure 2. The data shown in Figure 3 indicated that all $\Delta t_C$ values with $(NH_4)_2SO_4$ were greater than those without $(NH_4)_2SO_4$ regardless of the nanopore diameter. The mean values of $\Delta t_C$ with $(NH_4)_2SO_4$ and $\Delta t_C$ without $(NH_4)_2SO_4$ were 2.3 and 0.4 ms, respectively: the mean value of $\Delta t_C$ with $(NH_4)_2SO_4$ was approximately 5.8 times larger than that without $(NH_4)_2SO_4$. The figure also confirms that there was no significant correlation between the nanopore diameter and the dwell time in the diameter range of 1.68 to 1.97 nm. Only the dependence of the dwell time on the type of the aqueous solutions used (KCl aq or KCl + $(NH_4)_2SO_4$ aq) was clearly confirmed. As mentioned above, we believe that the surface state of the nanopore wall changed depending on the type of aqueous solutions used. If the interaction between poly(dT)$_{60}$ and the nanopore wall surface was a major factor in determining the dwell time, the dwell time would not change significantly even if the pore size somewhat changed (i.e., within 1.68 to 1.97 nm). This is thought to be because the structure of poly(dT)$_{60}$ is not straight but winding in aqueous solution, which enabled poly(dT)$_{60}$ to contact and interact with the nanopore wall surface even if the pore size increased to some extent. Needless to say, the dwell time is expected to be shorter if the pore diameter is much larger than 1.97 nm. Conversely, the dwell time is expected to be longer if the pore diameter is smaller than 1.67 nm and approaches the size where poly(dT)$_{60}$ can barely pass through.

Incidentally, we selected $(NH_4)_2SO_4$ instead of $NH_4Cl$ for our measurements because the conductance of the $(NH_4)_2SO_4$ aqueous solution is higher than that of the $NH_4Cl$ aqueous solution. (The measured conductance of each solution was $\sigma$(1 M $(NH_4)_2SO_4$) = 0.126 S/cm and $\sigma$(1 M $NH_4Cl$) = 0.104 S/cm.) An aqueous solution with a higher conductance is suitable for nanopore sensing because the amplitude of the current blockade increases, leading to a higher signal-to-noise ratio. However, as it stood, it was not possible to clearly determine whether the dwell time prolongation effect was caused by $NH_4^+$ or $SO_4^{2-}$. To clarify this, we will conduct experiments using an $NH_4Cl$ aqueous solution in future research.

The remainder of the study focused on dNTP translocation through nanopores. Figure 4 presents the data set of ionic


https://doi.org/10.1021/acsomega.3c02703
ACS Omega 2023, 8, 21285−21292

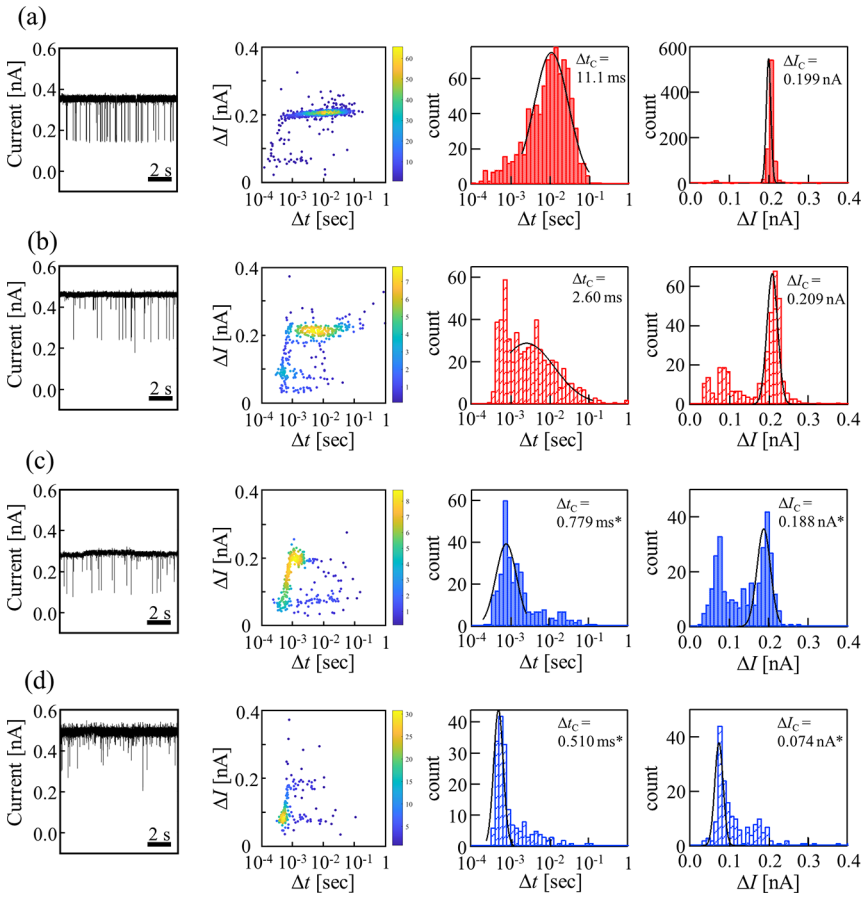


**Figure 4.** Ionic current blockades at 0.2 V when dCTP passed through nanopores. Each data set includes a time trace of the ionic current, a kernel density scatter plot of the ionic current blockade values ($\Delta I$) and dwell times ($\Delta t$), and histograms of $\Delta t$ and $\Delta I$. The histograms were fitted with Gaussian functions, and their central values were determined to be $\Delta t_C$ and $\Delta I_C$. (a) Data set when the nanopore formation and current blockade measurement were performed in a 0.5 M KCl + 0.5 M $(NH_4)_2SO_4$ aqueous solution. (b) Data set when the nanopore formation was performed in a 0.5 M KCl + 0.5 M $(NH_4)_2SO_4$ aqueous solution and the current blockade measurement was performed in a 1 M KCl aqueous solution. (c) Data set when the nanopore formation was performed in a 1 M KCl aqueous solution and the current blockade measurement was performed in a 0.5 M KCl + 0.5 M $(NH_4)_2SO_4$ aqueous solution. (d) Data set when the nanopore formation and current blockade measurement were performed in a 1 M KCl aqueous solution. *Note that the statics that rely on many events with $\Delta t$ of less than 0.5 ms are less reliable because the current was low-pass filtered with a cutoff frequency of 2 kHz. Especially, the data in (c) and (d) are derived from many events with $\Delta t$ of less than 0.5 ms, and the values of $\Delta t_C$ and $\Delta I_C$ with asterisks in (c) and (d) are less accurate than the others.

current blockades when dCTPs passed through the nanopores. The voltage applied was 0.2 V. Figure 4a shows the data when the nanopore formation and current blockade measurement were performed in the 0.5 M KCl + 0.5 M $(NH_4)_2SO_4$ aqueous solution. Figure 4b shows the data when the nanopore formation was performed in the 0.5 M KCl + 0.5 M $(NH_4)_2SO_4$ aqueous solution and the current blockade measurement was performed in the 1 M KCl aqueous solution. Figure 4c shows the data when the nanopore formation was performed in the 1 M KCl aqueous solution and the current blockade measurement was performed in the 0.5 M KCl + 0.5 M $(NH_4)_2SO_4$ aqueous solution. Figure 4d shows the data when the nanopore formation and current blockade measurement were performed in the 1 M KCl aqueous solution. Each figure shows the time trace of the ionic current, the scatter plot of $\Delta I$ and $\Delta t$, and the histograms of $\Delta I$ and $\Delta t$. The nanopore diameters used in each experiment were estimated to be 1.06 (Figure 4a), 1.32 (Figure 4b), 0.95 (Figure 4c), and 1.37 nm (Figure 4d).

A greater number of events with longer dwell times were observed when the nanopore formation was performed in the aqueous solution containing $(NH_4)_2SO_4$ than in the aqueous solution without $(NH_4)_2SO_4$: the $\Delta t_C$ shown in Figure 4a,b was approximately 5−20 times larger than the $\Delta t_C$ shown in Figure 4c,d.

Goto and Matsui et al. reported that some types of cations present in an aqueous solution during nanopore formation by dielectric breakdown were well absorbed on the wall of a SiN nanopore; those cations remained adsorbed even after displacement of the aqueous solution.[25,52] In addition, as noted above, the dwell time of DNA passing through nanopores was increased by the interactions between the adsorbed cations and DNA.[25] Considering these reports, it could be assumed that for the data shown in Figure 4a,b, $NH_4^+$ adsorbed on the wall of the nanopore and interacted with dCTP, prolonging its dwell time. On the other hand, for the data shown in Figure 4c, the aqueous solution did not contain $NH_4^+$ during nanopore formation, suggesting that less $NH_4^+$ was adsorbed on the wall of the nanopore, and thus the dwell time of dCTP was not significantly increased. For the data shown in Figure 4d, there was no $NH_4^+$ in the aqueous solution during both nanopore formation and current blockade measurement; thus, the dwell time of dCTP was not prolonged by $NH_4^+$. To summarize briefly, the above results suggested


https://doi.org/10.1021/acsomega.3c02703
ACS Omega 2023, 8, 21285−21292

that $NH_4^+$ was well adsorbed on a nanopore wall especially when the nanopore was fabricated by dielectric breakdown, and the adsorbed $NH_4^+$ interacted with DNA to lengthen the dwell time.

Regarding the ionic current blockade, more events with smaller $\Delta I$ were observed for the data shown in Figure 4c,d than for the data shown in Figure 4a,b. This could be because our nanopores and sampling conditions were not sufficient to adequately measure the current blockade events of short durations without attenuations. In this study, the detected currents were filtered with a relatively low cutoff frequency (2 kHz). This is because the nanopore membranes used in this study had a high capacitance. (A poly-Si layer is not an insulator and does not contribute to the capacitance reduction.) Therefore, the noise in the current was large when the current was measured using a filter with a high cutoff frequency, and it was difficult to pick out the small amplitude current blockade signals while distinguishing them from the noise. Figure S2 shows the comparisons of the time traces of ionic current blockades which were low-pass filtered with cutoff frequencies of 2 and 10 kHz. The figures confirmed that small amplitude signals were difficult to be picked out from the noise when a low pass filter with a cutoff frequency of 10 kHz was used. Especially, regarding the data for dATP (discussed later in Figure 5), there were almost no blockade signal visible

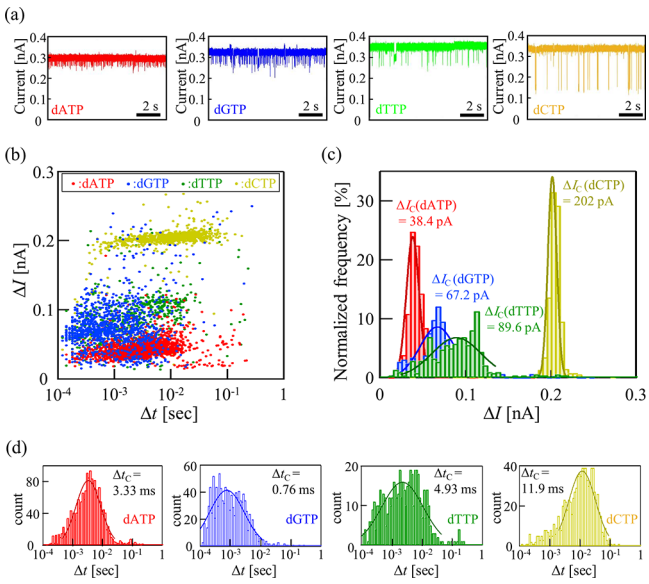


**Figure 5.** Ionic current blockades at 0.2 V when the four types of dNTPs passed through the same nanopore. (a) Time trace of the ionic current when each dNTP passed through the nanopores. (b) Scatter plot of the ionic current blockade values ($\Delta I$) and dwell times ($\Delta t$) for each dNTP translocation. (c) Normalized histogram of ionic current blockade values for each dNTP translocation. (d) Histograms of dwell times for each dNTP translocation.

at a cutoff frequency of 10 kHz. On the other hand, current blockade signals were clearly visible with a 2 kHz low pass filter. Consequently, we choose a 2 kHz low pass filter. However, the short current blockades with dwell times of less than 0.5 ms cannot be measured accurately at a cutoff frequency of 2 kHz. To measure both shorter and smaller signals accurately, it is necessary to measure the current using a low capacitance nanopore and a filter with a high cutoff frequency, which will be applied in a future work.

A comparison of the present study with previous literature examining the dwell time prolongation depending on the type of salt (electrolyte) is shown in Table 1. The dwell time ratio ($t_D/t_D$(KCl)) indicates how much longer the dwell time was compared to the case when KCl was used as an electrolyte. The dwell time prolongations by using LiCl and NaCl[32] were thought to be caused by the binding of $Li^+$ and $Na^+$ to DNA more strongly than $K^+$, which promoted neutralization of the DNA charge and weakened its electrophoretic mobility. The prolongations of the dwell times by using KGlu and NaGlu (using glutamate instead of chloride)[33] were attributed to the increase in viscosity of the solutions. The dwell time prolongations by using $CaCl_2$[25] and $(NH_4)_2SO_4$ (this work) were attributed to the interaction between the cation (i.e., $Ca^{2+}$ or $NH_4^+$) adsorbed on the nanopore wall surface and DNA.

Figure 5 presents the data set of ionic current blockades when the four types of dNTPs passed through the same nanopore in the 0.5 M KCl + 0.5 M $(NH_4)_2SO_4$ aqueous solution. (The nanopore used in this experiment was the same nanopore used to collect the experimental data shown in Figure 4a). Between each measurement, the nanopore was washed with 0.5 M KCl + 0.5 M $(NH_4)_2SO_4$ aqueous solution without dNTPs. Figure 5a shows the time trace of ionic current through the nanopore for each measurement. Clear ionic current blockades generated by the four types of dNTPs were observed. Figure 5b–d shows the scatter plot and histograms for each measurement. The kernel density scatter plot for the measurement of each dNTP is shown in Figure S3 in the Supporting Information.

The histogram of ionic current blockade values (Figure 5c) indicated that the four types of dNTPs could be statistically identified according to their blockade currents. The order and magnitude of $\Delta I_C$ was $\Delta I_C$(dATP) = 38.4 pA < $\Delta I_C$(dGTP) = 67.2 pA < $\Delta I_C$(dTTP) = 89.6 pA < $\Delta I_C$(dCTP) = 202 pA. The comparison of this result with the previous research reported by Yang et al.[26] is presented in Table 2. According to their report, the order and magnitude of the current blockades was $\Delta I_C$(dCTP) = 110 pA < $\Delta I_C$(dTTP) = 144 pA < $\Delta I_C$(dATP) = 146 pA < $\Delta I_C$(dGTP) = 179 pA. The order of the magnitude of $\Delta I_C$ was different between the two results. In addition, the ratios of $\Delta I_C$ between each dNTPs in this study were higher than those reported by Yang et al.[26] They also used a SiN nanopore as we did. However, in their experiment, dNTPs were drawn into nanopores by electroosmotic flow rather than by electrophoretic force by setting the applied voltage ($V_{trans}$(chamber without DNA) − $V_{cis}$(chamber with DNA)) at a negative value. In addition, they used a 1 M KCl aqueous solution without $(NH_4)_2SO_4$. On the other hand, in our experiment, dNTPs were drawn into nanopores by electrophoretic force by setting the applied voltage at a positive value in the 0.5 M KCl + 0.5 M $(NH_4)_2SO_4$ aqueous solution. These differences might be the reasons for the differences in the order and magnitude of the current blockades: their experiment and ours differed in terms of the density, distribution, and types of ions in the nanopore during each dNTP translocation.

As for the dwell time, the order of the dwell time of each dNTP was $\Delta t_C$(dGTP) = 0.76 ms < $\Delta t_C$(dATP) = 3.33 ms < $\Delta t_C$(dTTP) = 4.93 ms < $\Delta t_C$(dCTP) = 11.9 ms (Figure 5d). The reason for the difference in the dwell time of each dNTP could be the differences in the interaction forces between each dNTP and $NH_4^+$ adsorbed on the silanol groups of the nanopore wall surface: the dwell time was thought to become


https://doi.org/10.1021/acsomega.3c02703
ACS Omega 2023, 8, 21285−21292

Table 1. Dwell Time Prolongation when Using Salts Other than KCl[a]

| reference | type of salt | SiN membrane thickness (nm) | nanopore diameter (nm) | DNA | dwell time ratio ($t_D/t$(KCl)) |
|---|---|---|---|---|---|
| Kowalczyk *et al.*[32] | LiCl | 20 | 15−20 | ds(48.5 kbp), ss(7249 b) | 5−10 |
| Kowalczyk *et al.*[32] | NaCl | 20 | 15−20 | ds(48.5 kbp), ss(7249 b) | 1.5−2 |
| Plesa *et al.*[33] | KGlu | 20 | 10−20 | ds(20.7 kbp) | 3−6 |
| Plesa *et al.*[33] | NaGlu | 20 | 10−20 | ds(20.7 kbp) | 10−11 |
| Goto *et al.*[25] | $CaCl_2$ | 5 | 0.8−1.3 | ssDNA(82 b) | 10−100 |
| this work | $(NH_4)_2SO_4$ + KCl | 5 | 1.68−1.97 | ss(60 b) | 3−10 (ave. 5.8) |
| this work | $(NH_4)_2SO_4$ + KCl | 5 | 0.95−1.37 | dCTP | 5−20 |

[a]The dwell time ratio ($t_D/t_D$(KCl)) indicates how many times the dwell time increased compared to that when using KCl as an electrolyte. ds: double stranded, ss: single stranded.

Table 2. Ionic Current Blockade when each dNTP Passed through a Nanopore[a]

| reference | SiN nanopore thickness/diameter (nm) | applied voltage (mV) | driving force for DNA | $\Delta I$C(dCTP) (pA) | $\Delta I$C(dTTP) (pA) | $\Delta I$C(dATP) (pA) | $\Delta I$C(dGTP) (pA) |
|---|---|---|---|---|---|---|---|
| Yang *et al.*[26] | 10/1.8 | −500 | electroosmotic force | 110 | 144 | 146 | 179 |
| this work | 5/1.06 | 200 | electrophoretic force | 202 | 89.6 | 38.4 | 67.2 |

[a]The applied voltage is determined as $V_{trans}$(chamber without DNA) − $V_{cis}$(chamber with DNA).

longer as the interaction force between each dNTP and $NH_4^+$ became stronger.

The dwell times of dTTP and poly(dT)$_{60}$ were not significantly different. (The $\Delta t_C$ of poly(dT)$_{60}$ was approximately 1−5 ms, as shown in Figure 3.) One possible reason for this is considered as follows. Poly(dT)$_{60}$ has more areas that can interact with the nanopore wall surface than dTTP because of its longer length compared to dTTP. In addition, Poly(dT)$_{60}$ has more negative charges than dTTP. Therefore, the total adsorption force between Poly(dT)$_{60}$ and the nanopore wall surface was thought to be larger than that between dTTP and the nanopore wall surface due to the long length of Poly(dT)$_{60}$ compared to dTTP. On the other hand, the total force that poly(dT)$_{60}$ received from the electric field (i.e., electrophoretic force which drives DNA) was also larger than that dTTP received because Poly(dT)$_{60}$ has more negative charges than dTTP. As a result, the net forces on poly(dT)$_{60}$ and dTTP were thought to be not so different, leading to the similar dwell times.

## 4. CONCLUSIONS

We investigated the ionic current blockades when poly(dT)$_{60}$ or dNTPs passed through nanopores in an aqueous solution containing $(NH_4)_2SO_4$. Regarding the dwell time of poly(dT)$_{60}$, the mean value of $\Delta t_C$ measured in a 0.5 M KCl + 0.5 M $(NH_4)_2SO_4$ aqueous solution was significantly larger than that measured in a 1 M KCl aqueous solution without $(NH_4)_2SO_4$. This dwell time prolongation effect due to the aqueous solution containing $(NH_4)_2SO_4$ was also observed when dCTP passed through the nanopores.

In addition, when the nanopores were fabricated in an aqueous solution containing $(NH_4)_2SO_4$, the dwell time prolongation effect for dCTP still occurred even after the aqueous solution was displaced with the aqueous solution without $(NH_4)_2SO_4$. This result suggested one possible model for explaining the dwell time prolongation effect: $NH_4^+$ present in the aqueous solution during nanopore formation by dielectric breakdown was well absorbed on the nanopore surface, and $NH_4^+$ remained adsorbed even after displacement of the aqueous solution and interacted with dCTP to prolong its dwell time.

Furthermore, the ionic current blockades when the four types of dNTPs passed through the same nanopore were measured. The $\Delta I_C$ values for each dNTP were clearly separated, and the four types of dNTPs could be statistically identified according to their current blockade values.

In summary, the utilization of an aqueous solution containing $(NH_4)_2SO_4$ for SSN measurements prolonged the dwell time of DNA passing through nanopores and enabled the statistical identification of single nucleotides. Therefore, we believe that an aqueous solution containing $(NH_4)_2SO_4$ could be a promising solution for the realization of DNA sequencing with SSNs.

## ■ ASSOCIATED CONTENT

### Supporting Information

The Supporting Information is available free of charge at https://pubs.acs.org/doi/10.1021/acsomega.3c02703.

Scatter plot and histograms of ionic current-blockade values and dwell times when poly(dT)$_{60}$ passed through nanopores; time traces of ionic currents, which were low-pass filtered with cutoff frequencies of 2 and 10 kHz; and kernel density scatter plot of ionic current-blockade values and dwell times for each dNTP translocation through nanopores (PDF)

## ■ AUTHOR INFORMATION


### Corresponding Author

**Itaru Yanagi** − *Center for Exploratory Research, Research & Development Group, Hitachi, Ltd., Kokubunji, Tokyo 185-8603, Japan;* orcid.org/0000-0003-0218-4416; Email: itaru.yanagi.yr@hitachi.com

### Authors

**Rena Akahori** − *Center for Technology Innovation - Healthcare, Research & Development Group, Hitachi, Ltd., Kokubunji, Tokyo 185-8603, Japan*




https://doi.org/10.1021/acsomega.3c02703
ACS Omega 2023, 8, 21285−21292

**Ken-ichi Takeda** − *Center for Technology Innovation - Healthcare, Research & Development Group, Hitachi, Ltd., Kokubunji, Tokyo 185-8603, Japan*

Complete contact information is available at: https://pubs.acs.org/10.1021/acsomega.3c02703

### Notes

The authors declare no competing financial interest.

## ■ ACKNOWLEDGMENTS

We thank Dr. Yusuke Goto, Dr. Tatsuo Nakagawa, and Dr. Hai Huy Nguyen Pham of Hitachi for their valuable discussions and critical comments on the manuscript.

## ■ REFERENCES

(1) Feng, Y.; Zhang, Y.; Ying, C.; Wang, D.; Du, C. Nanopore-based Fourth-generation DNA sequencing technology. *Genomics, Proteomics Bioinf.* **2015**, *13*, 4−16.
(2) Deamer, D.; Akeson, M.; Branton, D. Three decades of nanopore sequencing. *Nat. Biotechnol.* **2016**, *34*, 518−524.
(3) Bhatti, H.; et al. Recent advances in biological nanopores for nanopore sequencing, sensing and comparison of functional variations in MspA mutants. *RSC Adv.* **2021**, *11*, 28996−29014.
(4) Mayer, S. F.; Cao, C.; Peraro, M. D. Biological nanopores for single-molecule sensing. *iScience* **2022**, *25*, No. 104145.
(5) Szalay, T.; Golovchenko, J. A. De novo sequencing and variant calling with nanopores using PoreSeq. *Nat. Biotechnol.* **2015**, *33*, 1087−1091.
(6) Jain, M.; et al. Nanopore sequencing and assembly of a human genome with ultra-long reads. *Nat. Biotechnol.* **2018**, *36*, 338−345.
(7) Bowden, R.; et al. Sequencing of human genomes with nanopore technology. *Nat. Commun.* **2019**, *10*, 1869.
(8) Akbari, V.; et al. Megabase-scale methylation phasing using nanopore long reads and NanoMethPhase. *Genome Biol.* **2021**, *22*, 68.
(9) Liu, L.; et al. Nanopore long-read-only metagenomics enables complete and high-quality genome reconstruction from mock and complex metagenomes. *Microbiome* **2022**, *10*, 209.
(10) Ferguson, S.; et al. Species-specific basecallers improve actual accuracy of nanopore sequencing in plants. *Plant Methods* **2022**, *18*, 137.
(11) Xue, L.; et al. Solid-state nanopore sensors. *Nat. Rev. Mater.* **2020**, *5*, 931−951.
(12) He, Y.; Tsutsui, M.; Zhou, Y.; Miao, X.-S. Solid-state nanopore systems: from materials to applications. *NPG Asia Mater.* **2021**, *13*, 48.
(13) Fried, J. P.; Swett, J. L.; Nadappuram, B. P.; Mol, J. A.; Edel, J. B.; Ivanov, A. P.; Yates, J. R. In situ solid-state nanopore fabrication. *Chem. Soc. Rev.* **2021**, *50*, 4974−4992.
(14) Wen, C.; Zhang, S. L. Fundamentals and potentials of solid-state nanopores: a review. *J. Phys. D: Appl. Phys.* **2021**, *54*, No. 023001.
(15) Meyer, N.; et al. Solid-state and polymer nanopores for protein sensing: A review. *Adv. Colloid Interface Sci.* **2021**, *298*, No. 102561.
(16) Fragasso, A.; Schmid, S.; Dekker, C. Comparing Current Noise in Biological and Solid-State Nanopores. *ACS Nano* **2020**, *14*, 1338−1349.
(17) Albrecht, T. Single-Molecule Analysis with Solid-State Nanopores. *Annu. Rev. Anal. Chem.* **2019**, *12*, 371−387.
(18) Goto, Y.; Akahori, R.; Yanagi, I.; Takeda, K. Solid-state nanopores towards single-molecule DNA sequencing. *J. Hum. Genet.* **2020**, *65*, 69−77.
(19) Lee, K.; et al. Recent Progress in Solid-State Nanopores. *Adv. Mater.* **2018**, *30*, 1704680.
(20) Taniguchi, M. Challenges of the practical applications of solid-state nanopore platforms for sensing biomolecules. *Appl. Phys. Express* **2022**, *15*, No. 070101.
(21) Liu, H.; Zhou, Q.; Wang, W.; Fang, F.; Zhang, J. Solid-State Nanopore Array: Manufacturing and Applications. *Small* **2023**, *19*, 2205680.
(22) Venta, K.; et al. Differentiation of Short, Single-Stranded DNA Homopolymers in Solid-State Nanopores. *ACS Nano* **2013**, *7*, 4629−4636.
(23) Feng, J.; et al. Identification of single nucleotides in $MoS_2$ nanopores. *Nat. Nanotechnol.* **2015**, *10*, 1070−1076.
(24) Goto, Y.; Yanagi, I.; Matsui, K.; Yokoi, T.; Takeda, K. Identification of four single-stranded DNA homopolymers with a solid-state nanopore in alkaline CsCl solution. *Nanoscale* **2018**, *10*, 20844−20850.
(25) Goto, Y.; Matsui, K.; Yanagi, I.; Takeda, K. Silicon nitride nanopore created by dielectric breakdown with a divalent cation: deceleration of translocation speed and identification of single nucleotides. *Nanoscale* **2019**, *11*, 14426−14433.
(26) Yang, H.; et al. Identification of Single Nucleotides by a Tiny Charged Solid-State Nanopore. *J. Phys. Chem. B* **2018**, *122*, 7929−7935.
(27) Lagerqvist, J.; Zwolak, M.; Di Ventra, M. Fast DNA sequencing via transverse electronic transport. *Nano Lett.* **2006**, *6*, 779−782.
(28) Farimani, A. B.; Min, K.; Aluru, N. R. DNA Base Detection Using a Single-Layer $MoS_2$. *ACS Nano* **2014**, *8*, 7914−7922.
(29) Fologea, D.; Uplinger, J.; Thomas, B.; McNabb, D. S.; Li, J. Slowing DNA Translocation in a Solid-State Nanopore. *Nano Lett.* **2005**, *5*, 1734−1737.
(30) Verschueren, D. V.; Jonsson, M. P.; Dekker, C. Temperature dependence of DNA translocations through solid-state nanopores. *Nanotechnology* **2015**, *26*, No. 234004.
(31) Wanunu, M.; Sutin, J.; McNally, B.; Chow, A.; Meller, A. DNA translocation governed by interactions with solid-state nanopores. *Biophys. J.* **2008**, *95*, 4716−4725.
(32) Kowalczyk, S. W.; Wells, D. B.; Aksimentiev, A.; Dekker, C. Slowing down DNA Translocation through a Nanopore in Lithium Chloride. *Nano Lett.* **2012**, *12*, 1038−1044.
(33) Plesa, C.; ávan Loo, N.; Dekker, C. DNA nanopore translocation in glutamate solutions. *Nanoscale* **2015**, *7*, 13605−13609.
(34) Wanunu, M.; Morrison, W.; Rabin, Y.; Grosberg, A. Y.; Meller, A. Electrostatic focusing of unlabelled DNA into nanoscale pores using a salt gradient. *Nat. Nanotechnol.* **2010**, *5*, 160−165.
(35) Akahori, R.; et al. Slowing single-stranded DNA translocation through a solid-state nanopore by decreasing the nanopore diameter. *Nanotechnology* **2014**, *25*, No. 275501.
(36) Larkin, J.; et al. Slow DNA Transport through Nanopores in Hafnium Oxide Membranes. *ACS Nano* **2013**, *7*, 10121−10128.
(37) Goto, Y.; Haga, T.; Yanagi, I.; Yokoi, T.; Takeda, K. Deceleration of single-stranded DNA passing through a nanopore using a nanometre-sized bead structure. *Sci. Rep.* **2015**, *5*, 16640.
(38) Squires, A. H.; Hersey, J. S.; Grinstaff, M. W.; Meller, A. A Nanopore−Nanofiber Mesh Biosensor To Control DNA Translocation. *J. Am. Chem. Soc.* **2013**, *135*, 16304−16307.
(39) Zhao, Y.; et al. Slowing down DNA translocation by a nanofiber meshed layer. *J. Phys. D: Appl. Phys.* **2018**, *51*, No. 045402.
(40) Tang, Z.; et al. Gel mesh as "brake" to slow down DNA translocation through solid-state nanopores. *Nanoscale* **2015**, *7*, 13207.
(41) Yoshida, H.; et al. Slowing the translocation of single-stranded DNA by using nano-cylindrical passage self-assembled by amphiphilic block copolymers. *Nanoscale* **2016**, *8*, 18270−18276.
(42) Keyser, U. F.; van der Does, J.; Dekker, C.; Dekker, N. H. Optical tweezers for force measurements on DNA in nanopores. *Rev. Sci. Instrum.* **2006**, *77*, 105105.
(43) De Vlaminck, I.; Henighan, T.; van Loenhout, M. T. J.; Burnham, D. R.; Dekker, C. Magnetic forces and DNA mechanics in multiplexed magnetic tweezers. *PLoS One* **2012**, *7*, No. e41432.
(44) Nelson, E. M.; Li, H.; Timp, G. Direct, Concurrent Measurements of the Forces and Currents Affecting DNA in a

Nanopore with Comparable Topography. *ACS Nano* **2014**, *8*, 5484−5493.
(45) Akahori, R.; et al. Discrimination of three types of homopolymers in single-stranded DNA with solid-state nanopores through external control of the DNA motion. *Sci. Rep.* **2017**, *7*, 9073.
(46) Wang, Y.-Q.; et al. Identification of Essential Sensitive Regions of the Aerolysin Nanopore for Single Oligonucleotide Analysis. *Anal. Chem.* **2018**, *90*, 7790−7794.
(47) Yanagi, I.; Ishida, T.; Fujisaki, K.; Takeda, K. Fabrication of 3-nm-thick $Si_3N_4$ membranes for solid-state nanopores using the poly-Si sacrificial layer process. *Sci. Rep.* **2015**, *5*, 14656.
(48) Yanagi, I.; Fujisaki, K.; Hamamura, H.; Takeda, K. Thickness-dependent dielectric breakdown and nanopore creation on sub-10-nm-thick SiN membranes in solution. *J. Appl. Phys.* **2017**, *121*, No. 045301.
(49) Yanagi, I.; Akahori, R.; Hatano, T.; Takeda, K. Fabricating nanopores with diameters of sub-1 nm to 3 nm using multilevel pulse-voltage injection. *Sci. Rep.* **2014**, *4*, 5000.
(50) Wanunu, M.; et al. Rapid electronic detection of probe-specific microRNAs using thin nanopore sensors. *Nat. Nanotechnol.* **2010**, *5*, 807−814.
(51) Yanagi, I.; Takeda, K. Sub-10-nm-thick SiN nanopore membranes fabricated using the $SiO_2$ sacrificial layer process. *Nanotechnology* **2021**, *32*, 415301.
(52) Matsui, K.; et al. Low-frequency noise induced by cation exchange fluctuation on the wall of silicon nitride nanopore. *Sci. Rep.* **2020**, *10*, 8662.



https://doi.org/10.1021/acsomega.3c02703
*ACS Omega* 2023, 8, 21285−21292